*J. Fluid Mech.* (2012), *vol.* 705, *pp.* 98–119. © Cambridge University Press 2012 
doi:10.1017/jfm.2012.116

# Vertical dispersion of model microorganisms in horizontal shear flow

**Takuji Ishikawa**†

Department of Bioengineering and Robotics, Tohoku University, 6-6-01, Aoba, Aramaki, Aoba-ku, Sendai 980-8579, Japan

(Received 24 April 2011; revised 6 February 2012; accepted 28 February 2012; first published online 13 April 2012)

Microorganisms often swim upwards due to the cell's phototaxis, chemotaxis or geotaxis, in flow fields with vertical velocity gradients. In this study, the vertical dispersion of model microorganisms was investigated under horizontal shear conditions. A microorganism was modelled as a spherical squirmer with or without bottom-heaviness. First, the three-dimensional movement of 100 identical squirmers in a homogeneous suspension was computed by the Stokesian dynamics method. The results show that the dispersion of squirmers is strongly affected by the swimming velocity and bottom-heaviness of the cells and the shear rate of the background flow. The vertical diffusion is considerably smaller than the horizontal diffusion. Interestingly, the vertical diffusion decreases as the volume fraction and the stresslet of squirmers decrease, which is opposite of the tendency in diffusion with no background flow. Next, a continuum model of a suspension of squirmers was developed using the diffusion tensor and the drift velocity to simulate the spatial distribution of squirmers in macroscopic flow fields. The results of the continuum model illustrate that the gyrotactic trapping found by Durham, Kessler & Stocker (*Science*, vol. 323, 2009, pp. 1067–1070) also appears in the present model considering cell–cell hydrodynamic interactions. In the case of horizontal Poiseuille flow, the volume fraction of bottom-heavy cells in the channel becomes considerably larger than that at the inlet. These fundamental findings are helpful for understanding the distribution of microorganisms in various water regimes in nature and industry.

**Key words:** micro-organism dynamics, suspensions, swimming/flying

## 1. Introduction

Microorganisms are distributed in various water regimes in nature and industry. Examples include plankton blooms in the ocean, bacterial digestion in sewage treatment and bioreactors for algae biofuels. In these environments, microorganisms often swim upwards, seeking the Sun's light for photosynthesis (phototaxis) and chemical substances, such as oxygen and nutrients, for metabolism (chemotaxis). The centre of mass of some species is displaced from the geometric centre, in a phenomenon called bottom-heaviness, which enables them to swim vertically upwards in a still fluid (Kessler 1986).

† Email address for correspondence: ishikawa@pfsl.mech.tohoku.ac.jp

https://doi.org/10.1017/jfm.2012.116 Published online by Cambridge University Press

The vertical swimming of microorganisms may be disturbed by a background flow field. Durham, Kessler & Stocker (2009) experimentally demonstrated that layers of high cell concentration were formed when the vertical migration of phytoplankton was disrupted by a horizontal shear. This mechanism may be responsible for the thin layers of phytoplankton commonly observed in the ocean. Although Durham *et al.* clarified the basic mechanism of layer formation, a theoretical understanding of the phenomena needs to be improved. Horizontal shear is especially important because the horizontal velocity in the ocean is often much larger than the vertical velocity. Horizontal shear flow is also important in many industrial situations. For example, Poiseuille flow in a horizontal channel is a typical engineering situation in which a strong vertical velocity gradient can easily be developed. In this study, we numerically investigated the vertical dispersion of model microorganisms under various horizontal shear conditions.

In the diffusion of cells in shear flow, there are two extreme conditions: (i) diffusion of swimming cells without background flow; and (ii) diffusion of inert particles in shear flow. In our previous study, we investigated the diffusion of model microorganisms (squirmers) in a semi-dilute suspension without background flow (Ishikawa & Pedley 2007). The results showed that the translational and rotational dispersion of squirmers were correctly described as diffusive processes over a sufficiently long time scale, although all of the movements of individual cells were calculated deterministically. The diffusion tensor is isotropic for non-bottom-heavy (NBH) cells, but anisotropic for bottom-heavy cells. If background shear is applied to the suspension, however, the diffusion tensor in no longer isotropic even for NBH cells. This effect is investigated in this paper.

The other extreme case, diffusion of inert particles in shear flow, has been investigated intensively. The shear-induced diffusion of non-Brownian and Brownian spheres in a concentrated suspension has been investigated numerically by Acrivos and coworkers (Wang, Murai & Acrivos 1998; Marchioro & Acrivos 2001; Drazer *et al.* 2002) and by Brady and coworkers (Morris & Brady 1996; Brady & Morris 1997; Foss & Brady 1999, 2000; Sierou & Brady 2004). They demonstrated that the non-zero components of the diffusion tensor were strongly dependent on the volume fraction of the spheres. These findings are useful for discussing cell motion under very strong shear, where the effect of cell swimming can be neglected. Under moderate or low shear conditions, however, the cells' motion becomes very different from that of inert particles. This effect will be clarified in this paper.

There are some experimental studies of the diffusivity of microorganisms. Childress, Levandowsky & Spiegel (1975) recognized that vertical cell swimming due to bottom-heaviness would lead to an anisotropic cell diffusivity tensor. Hill & Häder (1997) plotted horizontal and vertical projections of a large number of individual trajectories of bottom-heavy alga *Chlamydomonas nivalis* swimming in a fluid otherwise at rest. Vladimirov *et al.* (2000, 2004) used laser velocimetry to track a few hundred individual *C. nivalis* simultaneously. These results illustrated that the dispersion of cells can be described as a biased random walk. In these experiments, however, no background flow was imposed. The anisotropic property of the diffusion tensor in these studies was induced by the bottom-heaviness of cells, not by a background vorticity.

In this study, the vertical dispersion of model microorganisms was investigated under various horizontal shear conditions. A microorganism is modelled as a spherical

https://doi.org/10.1017/jfm.2012.116 Published online by Cambridge University Press

squirmer, with or without bottom-heaviness (Ishikawa, Simmonds & Pedley 2006). The details of the basic equations and numerical methods are explained in § 2. In § 3, the three-dimensional movement of 100 individual squirmers contained in a homogeneous suspension is computed by the Stokesian dynamics method. The effect of the swimming velocity and the bottom-heaviness of cells and the shear rate of the background flow on the dispersion of squirmers are discussed. Once the diffusion tensor and the drift velocity have been clarified, the results can be utilized to predict the spatial distribution of squirmers in macroscopic flow fields. Thus, in § 4, a continuum model of a suspension of squirmers is developed on the basis of the local equilibrium hypothesis, and the spatial distribution of squirmers in macroscopic flow fields is discussed. Two kinds of macroscopic flow fields were considered in this study: (*a*) two horizontal fluid layers flowing in opposite directions and (*b*) a horizontal Poiseuille flow between flat plates. Flow field (*a*) is examined in connection with the thin layer formation, and the Poiseuille flow is examined for its engineering applications. Horizontal Poiseuille flow has not been analysed in previous studies, and the spatial distribution of cells in this case is unclear.

## 2. Basic equations and numerical methods

### 2.1. *A squirmer*

The model microorganism used in this study is a spherical squirmer (Ishikawa *et al.* 2006). The squirmer is assumed to be neutrally buoyant, possibly bottom-heavy, non-Brownian and to swim at a very small Reynolds number. The sphere's surface is assumed to move purely tangentially, and these tangential motions are assumed to be axisymmetric and time-independent. The tangential surface velocity on a squirmer is given as follows:

$$\boldsymbol{u}_s = \sum_{n=1}^{2} \frac{2}{n(n+1)} B_n \left( \frac{\boldsymbol{e}\cdot\boldsymbol{r}\,\boldsymbol{r}}{r}\frac{}{r} - \boldsymbol{e} \right) P_n'(\boldsymbol{e}\cdot\boldsymbol{r}/r), \tag{2.1}$$

where $P_n$ is the $n$th Legendre polynomial, $\boldsymbol{e}$ is the unit orientation vector of a squirmer, $\boldsymbol{r}$ is the position vector and $r = |\boldsymbol{r}|$. A solitary squirmer swims with speed $U_{sol} = 2B_1/3$. We follow Ishikawa, Locsei & Pedley (2008) and omit squirming modes higher than the second (i.e. $B_n = 0$ when $n \geqslant 3$). We denote the ratio of second-mode squirming to first-mode squirming as $\beta$, i.e. $\beta = B_2/B_1$. Here $B_2$, and thus $\beta$, can have either sign. A squirmer with positive $\beta$ is a 'puller', whereas a squirmer with negative $\beta$ is a 'pusher'.

### 2.2. *Stokesian dynamics: motions of individual squirmers*

The Stokesian dynamics simulation method is used in § 3 to investigate the diffusion of individual squirmers in a homogeneous suspension. The Stokesian dynamics for computing the hydrodynamic interactions among an infinite suspension of squirmers, in the absence of Brownian motion and at negligible particle Reynolds number, was developed by Ishikawa *et al.* (2008). The numerical method used in this study is a slightly simplified version of the original method that neglects the far-field contribution of additional stresslets due to cell–cell interactions. The details of the method are explained in the following subsections. Its accuracy is confirmed in appendices A and B.

https://doi.org/10.1017/jfm.2012.116 Published online by Cambridge University Press

2.2.1. *Basic equations*

At negligible particle Reynolds number, the motions of $N$ squirmers periodically replicated in three-dimensional space can be given as (Ishikawa *et al.* 2008)

$$\begin{pmatrix} \boldsymbol{F} \\ \boldsymbol{L} \\ \boldsymbol{S} \end{pmatrix} = \left[ \boldsymbol{K}^{far} - \boldsymbol{K}_{2B}^{far} + \boldsymbol{K}_{2B}^{near} \right] \begin{pmatrix} \boldsymbol{U} - \boldsymbol{u} \\ \boldsymbol{\Omega} - \boldsymbol{\omega} \\ -\boldsymbol{E} \end{pmatrix} + \left[ \boldsymbol{K}^{far} - \boldsymbol{K}_{2B}^{far} \right] \begin{pmatrix} -\frac{2}{3} B_1 \boldsymbol{e} + \boldsymbol{Q}_{sq} \\ 0 \\ -\frac{1}{5} B_2 \, (3\boldsymbol{ee} - \boldsymbol{I}) \end{pmatrix} + \begin{pmatrix} \boldsymbol{F}_{sq}^{near} \\ \boldsymbol{L}_{sq}^{near} \\ \boldsymbol{S}_{sq}^{near} \end{pmatrix}, \tag{2.2}$$

where $\boldsymbol{F}$, $\boldsymbol{L}$ and $\boldsymbol{S}$ are the force, torque and stresslet a squirmer exerts on the fluid, respectively. Because the cells are neutrally buoyant, $\boldsymbol{F} = 0$ throughout this study. $\boldsymbol{U}$ and $\boldsymbol{\Omega}$ are the translational and rotational velocities of the squirmer, while $\boldsymbol{u}$ and $\boldsymbol{\omega}$ are the suspension average velocity and vorticity. Here $\boldsymbol{E}$ is the suspension average rate of strain tensor, $\boldsymbol{I}$ is the unit tensor and $\boldsymbol{Q}_{sq}$ is the far-field contribution of the irreducible quadrupole due to squirming motion; $\boldsymbol{K}^{far}$ is the far-field contribution to the grand resistance matrix, which is the inverse of the far-field contribution to the grand mobility matrix, i.e. $\boldsymbol{K}^{far} = \{\boldsymbol{M}^{far}\}^{-1}$; $\boldsymbol{M}^{far}$ is derived from the Faxén laws for the force, torque and stresslet for a squirmer, in which the disturbed flow field is expressed in terms of the multipole expansion of other squirmers. The infinite extent of the suspension is taken into account using Ewald summation (Beenakker 1986). To include near-field interactions, we add near-field multipoles in a pairwise additive fashion; $\boldsymbol{K}_{2B}^{far}$ is the far-field two-body resistance matrix and $\boldsymbol{K}_{2B}^{near}$ is the near-field two-body resistance matrix. The force, torque and stresslet generated by the two-squirmer interaction in the near-fluid, calculated numerically using the boundary element method (Ishikawa *et al.* 2006), are $\boldsymbol{F}_{sq}^{near}$, $\boldsymbol{L}_{sq}^{near}$ and $\boldsymbol{S}_{sq}^{near}$, respectively.

Equation (2.2) can be rewritten as

$$\left[ \boldsymbol{I} + \boldsymbol{M}_{FU}^{far} : \boldsymbol{K}_{FU}^{2b} \right] \cdot \begin{pmatrix} \boldsymbol{U} - \boldsymbol{u} - \frac{2}{3} B_1 \boldsymbol{e} + \boldsymbol{Q}_{sq} \\ \boldsymbol{\Omega} - \boldsymbol{\omega} \end{pmatrix} = \boldsymbol{M}_{FU}^{far} \cdot \left\{ \begin{pmatrix} \boldsymbol{F} + \boldsymbol{F}^{\alpha} \\ \boldsymbol{L} + \boldsymbol{L}^{\alpha} \end{pmatrix} - \boldsymbol{K}_{SU}^{2b} : \left[ -\boldsymbol{E} - \frac{1}{5} B_2 \, (3\boldsymbol{ee} - \boldsymbol{I}) \right] \right\} + \boldsymbol{M}_{SU}^{far} : \boldsymbol{S}^{far}, \tag{2.3}$$

where

$$\begin{pmatrix} \boldsymbol{F}^{\alpha} \\ \boldsymbol{L}^{\alpha} \end{pmatrix} = \boldsymbol{K}_{2B}^{near} : \begin{pmatrix} -\frac{2}{3} B_1 \boldsymbol{e} + \boldsymbol{Q}_{sq} \\ 0 \\ -\frac{1}{5} B_2 \, (3\boldsymbol{ee} - \boldsymbol{I}) \end{pmatrix} - \begin{pmatrix} \boldsymbol{F}_{sq}^{near} \\ \boldsymbol{L}_{sq}^{near} \end{pmatrix}. \tag{2.4}$$

The mobility and resistant matrices are split into four components as

$$\boldsymbol{M}^{far} = \begin{bmatrix} \boldsymbol{M}_{FU}^{far} & \boldsymbol{M}_{FE}^{far} \\ \boldsymbol{M}_{SU}^{far} & \boldsymbol{M}_{SE}^{far} \end{bmatrix}, \quad \boldsymbol{K}^{2b} = -\boldsymbol{K}_{2B}^{far} + \boldsymbol{K}_{2B}^{near} = \begin{bmatrix} \boldsymbol{K}_{FU}^{2b} & \boldsymbol{K}_{FE}^{2b} \\ \boldsymbol{K}_{SU}^{2b} & \boldsymbol{K}_{SE}^{2b} \end{bmatrix}, \tag{2.5}$$

where subscripts $FU, FE, SU$ and $SE$ indicate coupling between force and velocity, force and rate of strain, stresslet and velocity, and stresslet and rate of strain, respectively. Because $\boldsymbol{S}^{far}$ is a part of the problem in the original method,

https://doi.org/10.1017/jfm.2012.116 Published online by Cambridge University Press

equation (2.3) cannot be solved without coupling with another set of equations for the stresslet. To reduce the computational cost of the original method, while maintaining its accuracy, we simplified it by neglecting the effect of cell–cell interactions on the stresslet of squirmers in the far-field. Owing to this simplification, $\boldsymbol{S}^{far}$ may be approximated as

$$\boldsymbol{S}^{far} = -\boldsymbol{E} - \tfrac{1}{5}B_2\,(3\boldsymbol{ee} - \boldsymbol{I})\,. \tag{2.6}$$

Because the interaction effect is of order $c^2$, where $c$ is the volume fraction of cells, the stresslet due to cell–cell interactions becomes one order of magnitude smaller than the stresslet of a solitary cell by setting the range of $c$ used in this study to $c \leqslant 0.1$. A similar simplification was also discussed in Banchio & Brady (2003) for Brownian rigid spheres. The accuracy of the simplified method in calculating translational and rotational velocities of squirmers is still high. This was confirmed numerically by comparing the present method with the original method for two benchmark tests: (i) the interactions of three inert spheres in shear flow and (ii) diffusion of squirmers in a fluid otherwise at rest. The results of these benchmark tests are explicitly shown in appendices A and B.

If squirmers are bottom-heavy, external gravitational torques are generated when they are not oriented vertically. If the distance of the centre of gravity is $h$ from the centre of the squirmer, there is an additional torque of

$$\boldsymbol{L}_{bh} = \tfrac{4}{3}\pi a^3 \rho h \boldsymbol{e} \wedge \boldsymbol{g}, \tag{2.7}$$

where $\rho$ is the cell density, $\boldsymbol{g}$ is the gravitational acceleration vector and the gravitational direction $\boldsymbol{g}/g$ is taken as $-\boldsymbol{y}$ throughout this paper.

2.2.2. *Numerical procedures*

We calculate the interacting squirmers' motion in shear flow given by the rate of strain tensor and the vorticity as

$$\boldsymbol{E} = \frac{\dot{\gamma}}{2}\begin{pmatrix} 0 & 1 & 0 \\ 1 & 0 & 0 \\ 0 & 0 & 0 \end{pmatrix}, \quad \boldsymbol{\omega} = -\frac{\dot{\gamma}}{2}(0, 0, 1) \tag{2.8}$$

where $\dot{\gamma}$ is the shear rate. The $x$-axis is taken to be in the flow direction, $y$ is the direction with velocity gradient and $z$ is the vorticity direction. A suspension of infinite extent is represented by the periodic boundary conditions. Time marching is performed by the fourth-order Adams–Bashforth scheme. In a unit computational domain, we placed 100 squirmers with random initial positions and orientations. A short-range inter-particle repulsive force, as in Ishikawa *et al.* (2008), is added to the system to avoid the prohibitively small time step needed to overcome the problem of overlapping particles.

All equations are non-dimensionalized using the radius $a$, fluid viscosity $\mu$ and characteristic time $1/\omega_{max}$, where $\omega_{max}$ is the maximum vorticity. In the case of shear flow, $\omega_{max} = \dot{\gamma}/2$. There are two important dimensionless parameters in addition to $\beta$: $\Phi$ and $\Psi$ (Durham, Climent & Stocker 2011). Here $\Phi$ is the ratio of the swimming velocity of a solitary squirmer $U_{sol}$ to the characteristic velocity, defined as

$$\Phi = \frac{U_{sol}}{a\omega_{max}} \tag{2.9}$$

https://doi.org/10.1017/jfm.2012.116 Published online by Cambridge University Press

and $\Psi$ is the ratio of the viscous torque to the gravitational torque, defined as

$$\Psi = \frac{6\mu\omega_{max}}{\rho g h}. \tag{2.10}$$

The translational cell diffusivity is a measure of the increasing displacements between pairs of particles. If the mean square displacement grows linearly in time, the spread is diffusive. Thus, we calculate the mean square displacement $R^2$,

$$R^2(\Delta t) = \frac{1}{N}\sum_{n=1}^{N} \boldsymbol{R}_n^2(\Delta t) \tag{2.11}$$

where $N$ is the total number of particles, $\boldsymbol{R}_n(\Delta t) = \boldsymbol{r}_n(\Delta t) - \boldsymbol{r}_n(0)$ and $\boldsymbol{r}_n$ is the position vector of squirmer $n$. We show in § 3.1 that $R_y^2$ and $R_z^2$ of NBH squirmers grow linearly in time. When squirmers are bottom-heavy, on the other hand, they swim upwards on average. The drift velocity $U_d$ is defined as

$$\boldsymbol{U}_d = \lim_{\Delta t\to\infty} \frac{1}{N\Delta t}\sum_{n=1}^{N} \boldsymbol{R}_n(\Delta t). \tag{2.12}$$

To discuss the dispersion of bottom-heavy squirmers relative to the bulk motion, the mean square displacement relative to the bulk motion $\hat{R}^2$ is calculated as

$$\hat{R}^2(\Delta t) = \frac{1}{N}\sum_{n=1}^{N} \hat{\boldsymbol{R}}_n^2(\Delta t), \quad \hat{\boldsymbol{R}}_n(\Delta t) = \boldsymbol{R}_n(\Delta t) - \boldsymbol{U}_d\Delta t. \tag{2.13}$$

The diffusion tensor $\boldsymbol{D}$ is defined as

$$\boldsymbol{D} = \lim_{\Delta t\to\infty} \frac{1}{2N\Delta t}\sum_{n=1}^{N} \hat{\boldsymbol{R}}_n(\Delta t)\hat{\boldsymbol{R}}_n(\Delta t). \tag{2.14}$$

### 2.3. *A continuum model: macroscopic distribution of squirmers*

A continuum model of a suspension of squirmers is used in § 4 to simulate the spatial distribution of squirmers in macroscopic flow fields, in which the variables are volume-averaged quantities. In deriving the basic equations of the continuum model, we assume that the system is composed of subsystems where the rules of equilibrium apply (i.e. the local equilibrium hypothesis). In this case, the diffusion tensor and the drift velocity in the continuum model can be calculated from the Stokesian dynamics simulation, assuming a homogeneous suspension at equilibrium.

The conservation of cells in the continuum limit may be expressed by the advection–diffusion equation as

$$\frac{\partial c}{\partial t} = -\nabla\cdot[(\boldsymbol{V} + \boldsymbol{U}_d)\, c] + \nabla\cdot[\boldsymbol{D}\cdot\nabla c], \tag{2.15}$$

where $c$ is the volume fraction of squirmers (i.e. the volume of the cells divided by the combined volume of the fluid and cells), $\boldsymbol{V}$ is the background macroscopic flow velocity, $\boldsymbol{U}_d$ is the drift velocity of the squirmers and $\boldsymbol{D}$ is the diffusion tensor. We assume that $\boldsymbol{V}$ is unaffected by the cell concentration, which is a good approximation when the squirmers are neutrally buoyant and the cell concentration is not too large. The equation is again non-dimensionalized using the radius $a$, fluid viscosity $\mu$ and characteristic time $1/\omega_{max}$.

https://doi.org/10.1017/jfm.2012.116 Published online by Cambridge University Press

In § 4, we consider two kinds of macroscopic flow fields: (*a*) two horizontal fluid layers flowing in opposite directions and (*b*) a horizontal Poiseuille flow between flat plates. Flow field (*a*) is given by

$$\boldsymbol{V} = \left(2\delta \tanh \frac{y}{\delta}, 0, 0\right), \tag{2.16}$$

where $\delta$ controls the thickness of the strong shear region. The maximum shear rate of 2 is exerted at $y = 0$, where the shear rate is non-dimensionalized by $\omega_{max}$. This flow field was used to investigate the formation of thin layers of high cell concentration, as discussed in § 4.1. The same flow field was also used by Bearon, Hazel & Thorn (2011). Poiseuille flow between flat plates is given by

$$\boldsymbol{V} = \left(\frac{H}{2}\left[1 - \left(\frac{2y}{H}\right)^2\right], 0, 0\right), \tag{2.17}$$

where $H$ is the distance between the plates. The maximum shear rate of 2 is exerted on the wall (i.e. $y = \pm H/2$), where the shear rate is again non-dimensionalized by $\omega_{max}$. This flow field is presented in §§ 4.2 and 4.3. In both flows, the strength of the flow velocity relative to the swimming velocity of the cells is controlled by $\Phi$.

If we focus on a microscopic region in the large bulk flow, the velocity field may be approximated as a simple shear flow, because the higher-order velocity gradients of (2.16) and (2.17) become negligibly small. In this case, the effect of background flow on the microscopic region is simply represented by the shear rate $\dot{\gamma}$. Therefore, under the local equilibrium hypothesis, $\boldsymbol{U}_d$ and $\boldsymbol{D}$ in (2.15) become functions of only $c$, $\Phi$ and $\Psi$. Under given conditions for $c$, $\Phi$ and $\Psi$, $\boldsymbol{U}_d$ and $\boldsymbol{D}$ can be calculated by Stokesian dynamics, as explained in § 2.2. In this study, we compiled a database of $\boldsymbol{U}_d$ and $\boldsymbol{D}$ over the range $0 \leqslant c \leqslant 0.1$ and $0 \leqslant 1/\Phi \leqslant 5$, prior to the simulation. When simulating the continuum model, the $\boldsymbol{U}_d$ and $\boldsymbol{D}$ values in (2.15) are interpolated from the database, which is much more efficient than performing a Stokesian dynamics simulation at every time step.

We calculate the spatial distribution of squirmers by numerically solving (2.15). The diffusion term in (2.15) is discretized by the second-order finite volume method, and the advection term is discretized by the QUICK scheme (Leonard 1979) (i.e. the third-order upwind scheme). Time advancement is performed by the Euler explicit method. In § 4.1, one-dimensional analysis of thin layer formation is presented. In (2.16) $\delta$ is set equal to 100, and the computational region is $-500 \leqslant y \leqslant 500$ (cf. figure 8*a*). The mesh number in the $y$-direction is 2000. In § 4.2, one-dimensional analysis of a Poiseuille flow (equation (2.17)) is presented. We set $H$ equal to 100, and the mesh number in the $y$-direction is 200. In § 4.3, two-dimensional analysis of a Poiseuille flow is presented. We again set $H$ equal to 100 and the channel length is set equal to 4000. The mesh numbers in the $y$ and $x$ directions are 200 and 400, respectively.

## 3. Diffusion of individual squirmers in a homogeneous suspension

In this section, motions of individual squirmers in a homogeneous suspension under shear are calculated by the Stokesian dynamics method. Diffusion of both NBH and bottom-heavy squirmers was investigated.

### 3.1. *Diffusion of NBH squirmers*

The three-dimensional movement of 100 identical NBH squirmers with $\beta = 5$ in shear flow is computed with volume fraction $c = 0.1$ and $\Phi = 2$, using the Stokesian

https://doi.org/10.1017/jfm.2012.116 Published online by Cambridge University Press

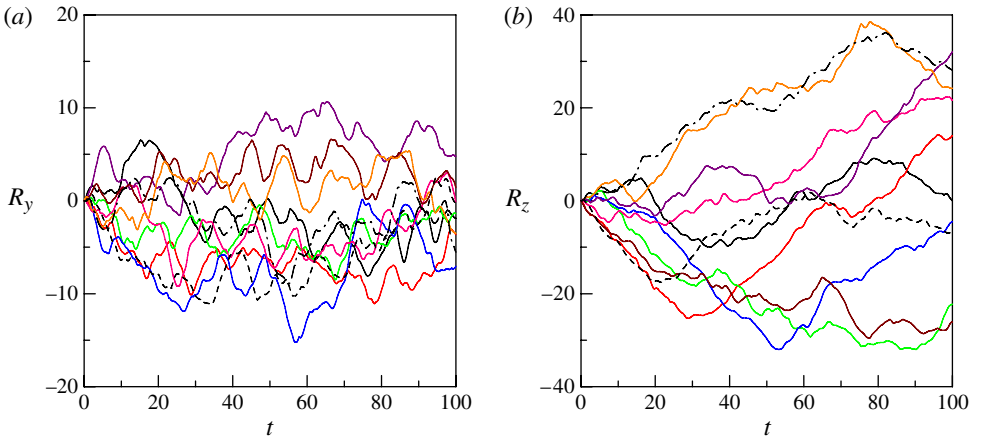



FIGURE 1. (Colour online available at journals.cambridge.org/flm) Displacements of 10 sample NBH squirmers with $\beta = 5$ for 100 time units ($c = 0.1$ and $\Phi = 2$): (*a*) displacement in the $y$ direction; and (*b*) displacement in the $z$ direction.

dynamics method. Figure 1 shows the displacement of 10 sample squirmers in the $y$ and $z$ directions for 100 time units. We see that the displacement in the $y$ direction is much smaller than that in the $z$ direction. Because the background shear generates vorticity in the $z$ direction, squirmers swimming in the $y$ direction rotate with the vorticity. Owing to this rotation, the $y$ position of the squirmers oscillates frequently (figure 1*a*). The displacements in the $z$ direction have larger oscillation wavelengths compared to those in the $y$ direction. Because the background vorticity does not directly contribute to the orientation change of squirmers relative to the $z$-axis, the squirmers can swim more smoothly in the $z$ direction.

The square displacement $R_y^2$ and $R_z^2$ were calculated from the trajectories of squirmers, and the results are shown in figure 2. The values of $R_y^2$ and $R_z^2$ with no background flow are also shown in the figure for comparison. We see that $R^2$ has slope 2 when $\Delta t < 1$, indicating that the motion of squirmers is ballistic on this short time scale. When $\Delta t > 100$, $R^2$ has slope 1, indicating that the motion of squirmers is diffusive on this longer time scale. The diffusion in the $y$ direction is considerably smaller than that in the $z$ direction. The diffusive property appears in a much shorter time ($\Delta t \approx 20$) in the $y$ direction than in the $z$ direction, because swimming in the $y$ direction is always disturbed by the background vorticity. We also found that the results with no background flow were very close to the square displacement in the $z$ direction under shear. This result illustrates that diffusion in the vorticity direction is not greatly affected by the background shear.

Next, the effect of the volume fraction $c$ was investigated. figure 3 shows the square displacement in the $y$ and $z$ directions with $c = 0.025, 0.05, 0.075$ and $0.1$ ($\beta = 5$ and $\Phi = 2$). Interestingly, the results of $R_y^2$ and $R_z^2$ show different tendencies: $R_z^2$ decreases as $c$ is increased, whereas $R_y^2$ increases as $c$ is increased. The mechanism of these different tendencies may be explained as follows. When there is no background vorticity, the changes in orientation due to hydrodynamic interactions, coupled with the propulsion of the squirmers, results in diffusion in space, with a translational diffusivity that is inversely proportional to the orientational diffusivity (Berg 1983). In the semi-dilute regime, the orientational diffusivity is proportional to $c$, and the

https://doi.org/10.1017/jfm.2012.116 Published online by Cambridge University Press

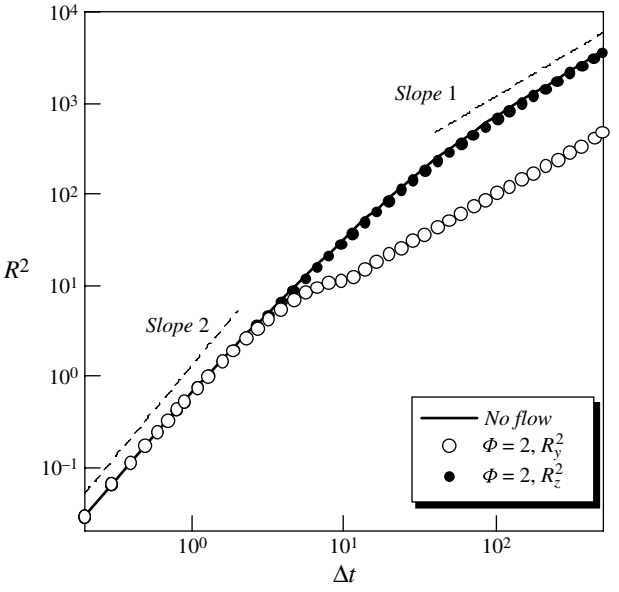



FIGURE 2. Square displacements of NBH squirmers with $\beta = 5$ ($c = 0.1$). *No flow* indicates the results with no background flow.

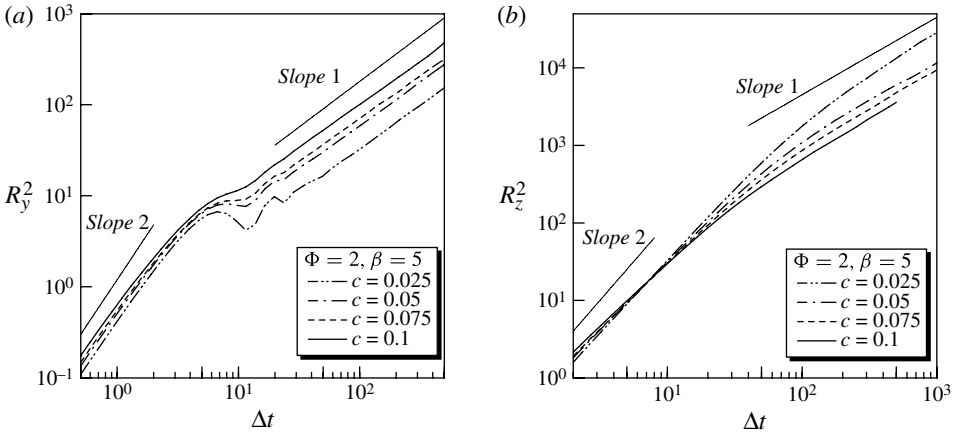



FIGURE 3. Effect of volume fraction $c$ on the square displacements of NBH squirmers ($\beta = 5$ and $\Phi = 2$): (*a*) square displacement in the $y$ direction; and (*b*) square displacement in the $z$ direction.

translational diffusivity is inversely proportional to $c$ (Ishikawa & Pedley 2007). In the case of shear flow, the background vorticity does not disturb the motion in the $z$-direction. Thus similar scaling may be applied to the diffusion in the $z$-direction, and $R_z^2$ tends to decrease as $c$ is increased.

The increase in $R_y^2$ with $c$ can be explained as follows. If a solitary NBH squirmer swims in shear flow, it rotates with a constant background vorticity in the $z$ direction. In this case, the $y$ position of the squirmer oscillates, but there is no net displacement

https://doi.org/10.1017/jfm.2012.116 Published online by Cambridge University Press

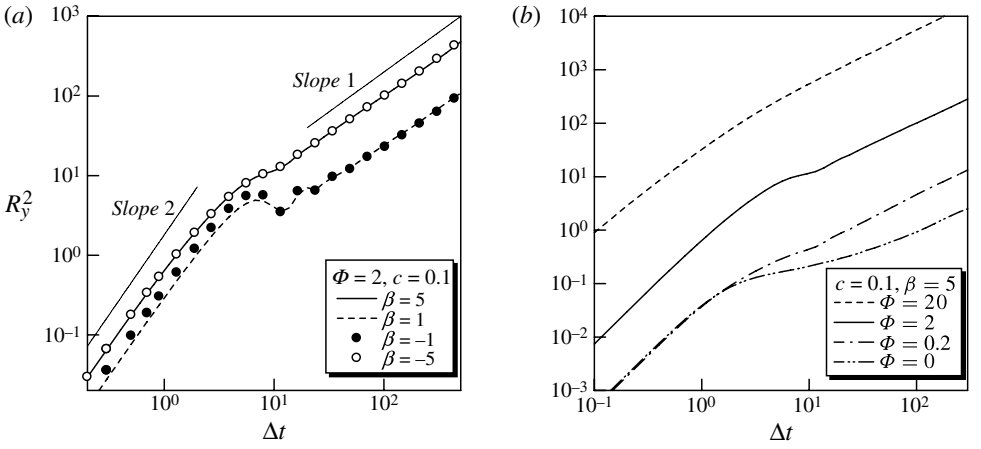



FIGURE 4. Effect of second-mode squirming $\beta$ and $\Phi$ on the square displacements ($c = 0.1$): ($a$) effect of $\beta$ ($\Phi = 2$); and ($b$) effect of $\Phi$ ($\beta = 5$).

in the $y$ direction over the long run. This tendency is totally different from that of the $z$ direction when a cell swims with a constant velocity. Therefore, when discussing diffusion in the $y$ direction, the aforementioned scaling argument has to be modified. The translational diffusivity in the $y$ direction is proportional to $L_c^2/t_c$, where $L_c$ and $t_c$ denote the typical displacement in the $y$ direction due to collision of squirmers and typical time between collisions, respectively. In the dilute limit, $t_c$ approaches infinity, because no collision occurs. As $c$ is increased, $t_c$ is decreased while keeping $L_c$ almost constant. Thus, the diffusivity in the $y$ direction increases as $c$ is increased, and $R_y^2$ also increases with $c$. These results illustrate that the diffusion tensor of swimming cells under shear is anisotropic not only quantitatively but also qualitatively in terms of the response to the change in volume fraction.

The disturbing flow field is also strengthened by increasing the second-mode squirming, i.e. $|\beta|$, because the stresslet of a solitary squirmer is proportional to $\beta$, and the velocity disturbance in the far-field is dominated by the stresslet. Thus, $R_y^2$ may be increased by increasing $|\beta|$. The effect of $\beta$ on $R_y^2$ is shown in figure 4($a$). We can see that $R_y^2$ increases as $|\beta|$ is increased, as predicted by the mechanism explained in the previous paragraph. The difference in the sign of $\beta$ on $R_y^2$ is small. These results indicate that the diffusion of squirmers in the $y$-direction is determined by the strength of the stresslet, but the sign of the stresslet (i.e. pusher or puller) is unimportant. On the other hand, $R_z^2$ decreases as $|\beta|$ is increased (data not shown). This tendency is again opposite to that of $R_y^2$, but the same as that for square displacement with no background flow (cf. Ishikawa & Pedley 2007).

Another important parameter is $\Phi$, which indicates the strength of the swimming velocity relative to the shear flow. When $\Phi$ approaches infinity (i.e. there is no background shear), the results are equivalent to those of our earlier study on the diffusion of squirmers in a fluid otherwise at rest (Ishikawa & Pedley 2007). When $\Phi$ is zero, (i.e. there is no swimming), the results are equivalent to those of our earlier study on shear-induced diffusion of non-Brownian spheres (Ishikawa & Yamaguchi 2008). When $\Phi$ is moderate, $R_y^2$ varies as shown in figure 4($b$) ($c = 0.1$ and $\beta = 5$). Here $R_y^2$ increases as $\Phi$ is increased. This is because a squirmer with larger $\Phi$ can

https://doi.org/10.1017/jfm.2012.116 Published online by Cambridge University Press

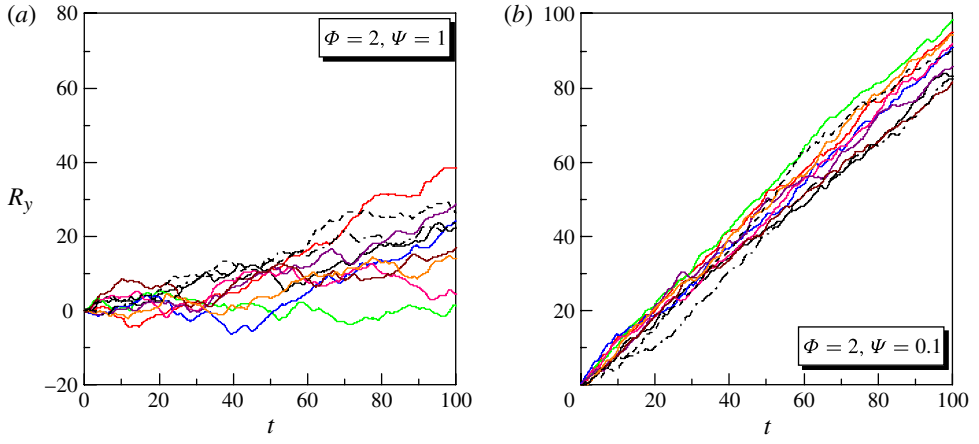



FIGURE 5. (Colour online) Vertical displacements of 10 sample bottom-heavy squirmers in horizontal shear flow for 100 time units ($\beta = 5$, $c = 0.1$ and $\Phi = 2$): (*a*) $\Psi = 1$; and (*b*) $\Psi = 0.1$.

swim a longer distance in a given time unit, and hence $R_y^2$ increases more rapidly as $\Phi$ is increased. It turns out that even small values of $\Phi$, such as $\Phi = 0.2$, dramatically increase the diffusion in the $y$ direction.

### 3.2. *Vertical diffusion of bottom-heavy squirmers*

In this section, the effect of bottom-heaviness on the vertical diffusion is discussed. The gravitational direction is taken as $-\boldsymbol{y}$, i.e. the direction of the negative velocity gradient. Thus, $\hat{R}_y^2$ indicates vertical square displacement, and the background shear is applied in the horizontal direction. Two parameter values ($\Psi = 1$ and 0.1) are used in this section, which defines the strength of bottom-heaviness.

The three-dimensional movement of 100 identical bottom-heavy squirmers with $\Psi = 1$ and 0.1 in horizontal shear flow was computed by the Stokesian dynamics method ($\beta = 5$, $c = 0.1$ and $\Phi = 2$). Figure 5 shows the displacement of 10 sample squirmers in the $y$ directions for 100 time units. We see that the bottom-heavy squirmers swim upwards, on average. The upward swimming velocity is large in the $\Psi = 0.1$ case, because the strong bottom-heaviness forces the squirmers to be oriented vertically upward. The upward drift velocity of squirmers in the $\Psi = 1$ case is about $U_d = 0.19$, and that in the $\Psi = 0.1$ case is about $U_d = 0.90$. The drift velocity is strongly influenced by the bottom-heaviness.

Figure 6 shows the square displacements $\hat{R}_y^2$ and $R_z^2$ in this case ($\beta = 5$, $c = 0.1$ and $\Phi = 2$). Here $\hat{R}_y^2$ becomes proportional to $\Delta t$ after a sufficiently long time. This indicates that the dispersion of bottom-heavy squirmers in the vertical direction, relative to the bulk motion, can be described by diffusion. The dependence of vertical diffusion on $\Psi$ seems to be complex: vertical diffusion increases from $\Psi = 0.1$ to 1 but decreases from $\Psi = 1$ to $\infty$, i.e. NBH cells. This may be explained as follows. In large $\Psi$ cases, the effect of background vorticity is so large that the squirmers continuously rotate around the same $y$ position, resulting in little increase in $\hat{R}_y^2$ over the long run. In small $\Psi$ cases, on the other hand, the effect of bottom-heaviness is so large that the squirmers constantly swim vertically upward. The fluctuation in the vertical velocity is small in this case, again resulting in little increase in $\hat{R}_y^2$ over

https://doi.org/10.1017/jfm.2012.116 Published online by Cambridge University Press

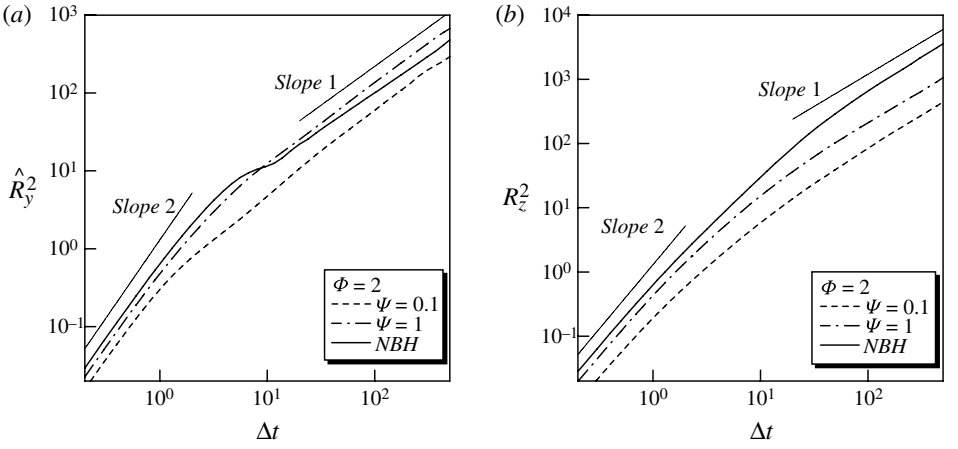



FIGURE 6. Effect of $\Psi$ on the square displacements ($\beta = 5$, $c = 0.1$ and $\Phi = 2$): (*a*) square displacement in the $y$ direction; and (*b*) square displacement in the $z$ direction. NBH indicates non-bottom-heavy squirmers.

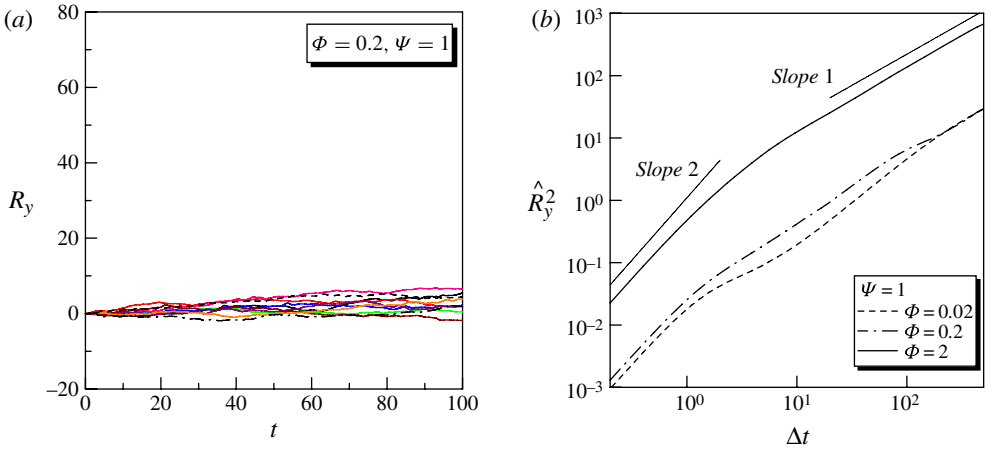



FIGURE 7. (Colour online) Effect of $\Phi$ on the vertical diffusivity ($\beta = 5$, $c = 0.1$, and $\Psi = 1$): (*a*) vertical displacements of 10 sample bottom-heavy squirmers with $\Phi = 0.2$; and (*b*) effect of $\Phi$ on the square displacement.

the long run, even though the drift velocity itself is large. In moderate $\Psi$ cases, the effects of background vorticity and bottom-heaviness are levelled, and the squirmers no longer swim steadily upward nor rotate continuously. The trajectories of these cells become erratic (cf. figure 5*a*), resulting in large values of $\hat{R}_y^2$ over the long run. Thus, $\hat{R}_y^2$ becomes larger with $\Psi = 1$ than with $\Psi \ll 1$ or $1 \ll \Psi$. Here $R_z^2$ monotonically decreases as $\Psi$ is decreased. This is because squirmers tend to orient vertically upwards when $\Psi$ is small, and the movement in the $z$ direction is suppressed. These results illustrate that the dispersion of squirmers is strongly affected by the bottom-heaviness of the cells and the shear rate of the background flow.

Finally, the effect of $\Phi$ on the vertical diffusivity was investigated. Figure 7(*a*) shows the displacement of 10 sample squirmers in the $y$ direction under the

https://doi.org/10.1017/jfm.2012.116 Published online by Cambridge University Press

| *Shear rate* | $\Phi$ | $\Phi\Psi$ | $U_{d,y}/U_{sol}$ | $D_{yy}/(aU_{sol})$ |
|---|---|---|---|---|
|  | 0 | 0.2 | 0.00 | $\infty$ |
| | 0.1 | 0.2 | 0.04 | 0.3 |
| | 1 | 0.2 | 0.13 | 0.3 |
| | 10 | 0.2 | 0.90 | 0.3 |
| | $\infty$ | 0.2 | 0.91 | 1.0 |

TABLE 1. Vertical drift velocity $U_{d,y}$ and vertical diffusivity $D_{yy}$ of bottom-heavy squirmers. Here $a$ is the radius of cells and $U_{sol}$ is the swimming velocity of cells. The shear rate increases as $\Phi$ is decreased, which is schematically represented by the black triangle ($\beta = 5$ and $c = 0.1$).

condition $\Phi = 0.2$ and $\Psi = 1$ ($\beta = 5$ and $c = 0.1$). By comparison with the case $\Phi = 2$ and $\Psi = 1$ (cf. figure 5*a*), we can see that the vertical displacement is reduced considerably when $\Phi = 0.2$. Because the swimming velocity of the squirmers is small when $\Phi$ is small, the vertical displacement is also small. The effect of $\Phi$ on the vertical square displacement is shown in figure 7(*b*). We see that when $\Phi = 2$, $\hat{R}_y^2$ is one order of magnitude larger than when $\Phi = 0.2$ and 0.02, although the results for $\Phi = 0.2$ and 0.02 are not very different. Thus, the effect of cell swimming on the vertical diffusivity can be neglected when $\Phi \leqslant 0.2$. The vertical drift velocity is about 0.001 when $\Phi = 0.02$ and about 0.013 when $\Phi = 0.2$. These results illustrate that the dispersion of bottom-heavy squirmers is strongly affected by the swimming velocity of the cells and the shear rate of the background flow.

## 4. Distribution of squirmers in macroscopic flow fields

In this section, we discuss the spatial distribution of squirmers in macroscopic flow fields. Before going into a detailed analysis, we first briefly explain the basic tendencies of the vertical drift velocity $U_{d,y}$ and the vertical diffusivity $D_{yy}$ with respect to the shear rate. The results for $U_{d,y}$ and $D_{yy}$ under the condition $\Phi\Psi = 0.2$ are listed in table 1 as an example ($\beta = 5$ and $c = 0.1$). The reason why $\Phi\Psi$ is kept as a constant is because this represents keeping cell properties the same and only varying the shear. In the table, the shear rate increases as $\Phi$ is decreased, and this is schematically represented by the black triangle. A $\Phi$ of 0 indicates an asymptotic value approaching an infinitely large shear rate and a $\Phi$ of '$\infty$' indicates the condition of no background flow. We can infer from the table that the vertical diffusivity is small when the shear rate is moderate, and the value varies little over the range $\Phi = 0.1$–10. The vertical drift velocity is strongly suppressed by increasing the shear rate, and the value is almost zero in the regime $\Phi \leqslant 0.1$. These results indicate that vertical diffusion dominates the vertical dispersion of the cells when the shear rate is sufficiently large, while the drift velocity dominates the vertical dispersion when the shear rate is sufficiently small. Such tendencies should affect the spatial distribution of squirmers in macroscopic flow fields. In this section, we investigated the spatial distribution of squirmers in the continuum limit under three kinds of conditions. The continuum model used in this section is explained in § 2.3.

https://doi.org/10.1017/jfm.2012.116 Published online by Cambridge University Press

### 4.1. *Formation of thin layers*

Durham *et al.* (2009) demonstrated experimentally that layers of high cell concentration are formed when the vertical migration of phytoplankton was disturbed by hydrodynamic shear. They developed a continuum model of cell concentration and showed that the gyrotactic trapping mechanism is responsible for the thin layers of phytoplankton commonly observed in the ocean. In their analysis, the background flow was assumed to be turbulent, and uniform eddy diffusivity was added to the system. Bearon *et al.* (2011) also investigated the formation of phytoplankton thin layers by using both the individual-based discrete model and the continuum model. However, cell–cell hydrodynamic interactions were not taken into account in these studies. In this section, we consider whether or not our numerical model can also explain the formation of thin layers of bottom-heavy squirmers. Although the volume fraction of cells used in this simulation may be larger than that of typical plankton blooms occurring in the ocean, such a volume could appear in many industrial settings.

As in Durham *et al.* (2009) and Bearon *et al.* (2011), the background velocity is given by (2.16) (as shown in figure 8*a*), and the flow is to the right in the upper layer and to the left in the lower layer. The background velocity is purely horizontal and the $y$-axis is chosen to point vertically upward. Let the cells be initially homogeneously distributed with a volume fraction of $c = 0.02$. The subsequent motion of the cells is simulated. The computational region is $-500 \leqslant y \leqslant 500$. At $y = -500$, a constant cell concentration of $c = 0.02$ is assumed. At $y = 500$, free stream conditions are specified. Although the geometric and kinematic parameters of real microorganisms vary quite widely, we use $\Phi\Psi = 0.2$ as an example. A solitary cell with $\Phi\Psi = 0.2$ rotates continuously due to the background vorticity if $\Phi < 0.2$. We note that the conclusions obtained in the following discussion are qualitatively unaffected by the selection of the parameter $\Phi\Psi$.

The results for concentration distributions with $\Phi = 0.4, 0.2$ and $0.1$ are shown in figure 8(*b–d*). When $\Phi = 0.4$, a slight increase in the concentration is observed around $y = 0$, and the results reach a steady state before $t = 1875$. Thin layer formation is not clearly observed in this case. When $\Phi = 0.2$, on the other hand, a layer of high concentration clearly appears around $y = -50$. A layer of low concentration also appears around $y = 100$. The computation is stopped at $t = 1170$, when the maximum concentration reaches 0.1, although the concentration distribution does not reach a steady state. The mechanism of thin layer formation can be explained as follows. The cells in the region $y < -100$ can swim steadily upwards because the shear rate is small and the vertical drift velocity is large. The cells in the region $y \approx -50$, on the other hand, may remain at about the same vertical position for a long time because of the high shear and the small vertical drift velocity. Thus, the cells in the $y < -100$ region accumulate toward $y = -50$, even though the cell concentration was initially homogeneous. This accumulation results in the formation of a horizontal layer of high cell concentration. The mechanism of thin layer formation with low cell concentration is also straightforward, and here cells are not supplied from the lower fluid but escape toward the upper fluid.

When $\Phi = 0.1$ (cf. figure 8*d*), a layer of high concentration again clearly appears around $y = -100$, whereas a layer of low concentration appears around $y = 150$. The computation is stopped at $t = 122$, when the maximum concentration reaches 0.1. The reason why the layer of high concentration appears at a lower $y$ position than in the $\Phi = 0.2$ case can be explained as follows. The shear rate with $\Phi = 0.1$ is twice as high as the shear rate with $\Phi = 0.2$ at the same $y$ position. Thus, the cells in the region $y \approx -100$ experience larger shear in the $\Phi = 0.1$ case than in the $\Phi = 0.2$ case. These cells remain near $y \approx -100$ for a long time, although the cells are able

https://doi.org/10.1017/jfm.2012.116 Published online by Cambridge University Press

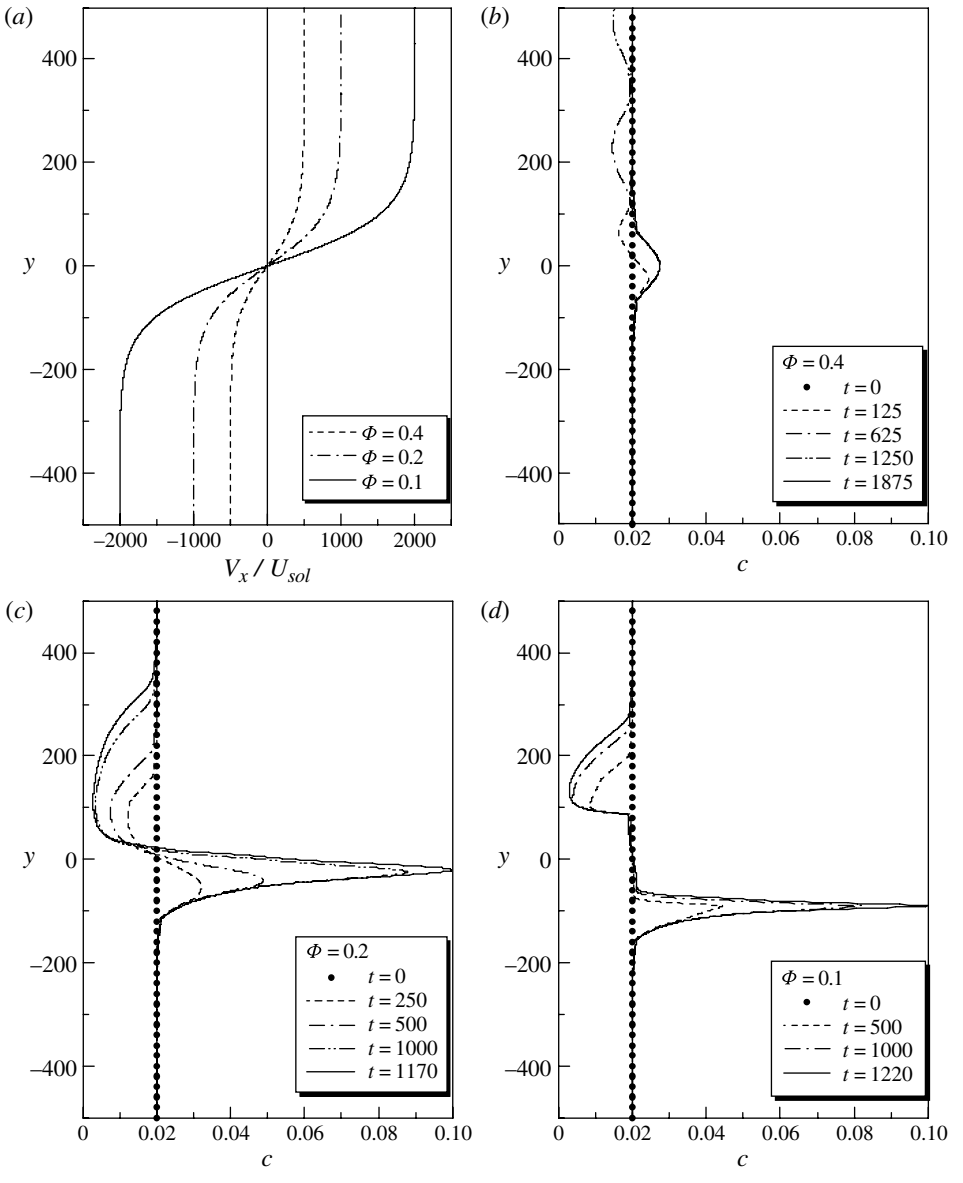



FIGURE 8. Analysis of thin layer formation ($\beta = 5$ and $\Phi\Psi = 0.2$): (*a*) velocity distributions with $\Phi = 0.1, 0.2$ and $0.4$, where $V_x$ is normalized by $U_{sol}$; (*b–d*) show changes in the concentration distribution over time with $\Phi = 0.4$, $0.2$ and $0.1$, respectively.

to swim steadily upward when $\Phi = 0.2$. This difference in squirmer behaviour results in layer formation at a lower $y$ position when $\Phi = 0.1$. These results illustrate that the gyrotactic trapping found by Durham *et al.* (2009) also appears in our study considering cell–cell hydrodynamic interactions.

### 4.2. *One-dimensional horizontal Poiseuille flow between flat plates*

In engineering applications, the spatial distribution of cells in channel flows would be important. Here, we investigated the distribution of squirmers in one-dimensional

https://doi.org/10.1017/jfm.2012.116 Published online by Cambridge University Press

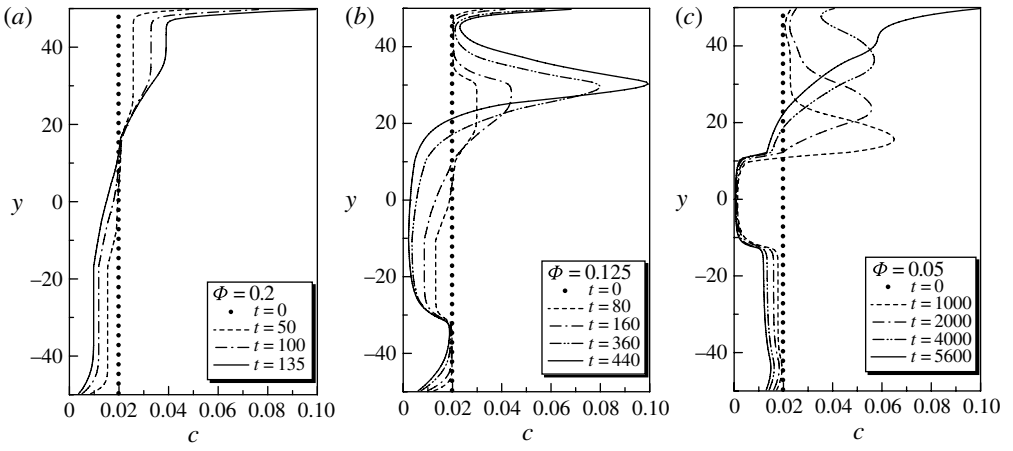



FIGURE 9. Changes in the concentration distributions over time in a one-dimensional horizontal Poiseuille flow ($\beta = 5$ and $\Phi\Psi = 0.2$): (*a*) $\Phi = 0.2$; (*b*) $\Phi = 0.125$; and (*c*) $\Phi = 0.05$.

horizontal Poiseuille flow between flat plates. Horizontal Poiseuille flow has not been analysed in previous studies using a continuum model based on individual cellular behaviour. The background velocity is given by (2.17). Let the cells be initially homogeneously distributed with a volume fraction $c = 0.02$. The subsequent motion of the cells is simulated. The computational region is $-50 \leqslant y \leqslant 50$. At $y = \pm 50$, the no-cell-flux condition is specified. In this section, we again use the condition $\Phi\Psi = 0.2$ as an example. A solitary cell with $\Phi\Psi = 0.2$ rotates continuously due to the background vorticity if $\Phi < 0.2$. The threshold $y$ position, where the solitary cell rotates continuously in the Poiseuille flow, is $y_{th} = \pm 2.5H\Phi$.

The results for concentration distributions with $\Phi = 0.2, 0.125$ and $0.05$ are shown in figure 9. In all cases, the computations are stopped when the maximum concentration reaches 0.1. If we continue these computations for a long enough time, the concentration distribution may eventually have only two layers, with $c \approx 1$ on top and $c \approx 0$ at the bottom. We do not investigate such long-run phenomena because the local concentration becomes unrealistically high. Moreover, the concentration may rapidly increases in the computational mesh next to the upper wall, because the cells accumulate locally under the no-cell-flux boundary condition. We do not focus on such a thin boundary layer and use the mesh number of 200 in the $y$ direction (cf. § 2.3). This is because the boundary layer near the upper wall has little effect on the bulk concentration distribution, and the finite mesh size is useful to sustain moderate computational time before reaching $c = 0.1$. When $\Phi = 0.2$, the threshold $y$ position is $y_{th} = \pm 50$. The cells near the walls have small drift velocities, whereas the cells that are farther away from the walls have large drift velocities. Thus, most of the cells swim steadily upward and tend to accumulate near the upper wall. When $\Phi = 0.125$, $y_{th} \approx \pm 31$. Thus, the cells in the region $-31 \leqslant y \leqslant 31$ tend to accumulate around $y \approx 31$, and a thin layer of high concentration develops at $t = 440$. A thin layer of high concentration is also formed near the upper wall. If we continue the computations for a much longer time, these two layers may merge near the upper wall, but this was not investigated. When $\Phi = 0.05$, $y_{th} \approx \pm 12$. The layer of low concentration thus appears in the region $-12 \leqslant y \leqslant 12$. A layer of high concentration is initially formed

https://doi.org/10.1017/jfm.2012.116 Published online by Cambridge University Press

at around $y = 15$ but gradually moves toward the upper wall. When $t = 5600$, the layer of high concentration is observed only near the upper wall. These results illustrate the fact that changes in the cell distribution over time are strongly affected by the velocity of the Poiseuille flow.

### 4.3. *Two-dimensional horizontal Poiseuille flow between flat plates*

In this section, we discuss the two-dimensional distribution of squirmers in a horizontal Poiseuille flow between flat plates. The background velocity is again given by (2.17), and the computational region is $0 \leqslant x \leqslant 4000$ and $-50 \leqslant y \leqslant 50$. At the inlet ($x = 0$), a homogeneous concentration of $c = 0.02$ is specified as a boundary condition. Free stream conditions are specified at the outlet and no-cell-flux conditions on the walls. At $t = 0$, no cells are present inside the computational region (i.e. $c = 0$), and subsequent changes in the concentration field with respect to time are simulated. We again do not focus on the thin boundary layer near the upper wall, and use the mesh number of 200 in the $y$ direction. We also assume that $\Phi\Psi = 0.2$, as in §§ 4.1 and 4.2.

The results for concentration distributions with $\Phi = 0.167, 0.125$ and $0.05$ at $t\Phi = 100$ are shown in figure 10. The concentration flux from the outlet is shown in figure 11 for each of these cases, where the concentration flux is defined by

$$q_{out} = \frac{\displaystyle\int_{-H/2}^{H/2} c_{out} V_{x,out}\, \mathrm{d}y}{\displaystyle\int_{-H/2}^{H/2} V_{x,out}\, \mathrm{d}y}. \tag{4.1}$$

The subscript *out* indicates the value at the outlet. Because the inlet concentration flux is fixed by the boundary conditions, $q_{out}$ should be 0.02 in the steady state. We can see from figure 11 that $q_{out}$ is slightly less than 0.02, even at $t\Phi = 100$, which indicates that the concentration field is still undergoing small developments. The computations are stopped at $t\Phi = 100$, when the maximum concentration in the $\Phi = 0.167$ case reaches 0.1, although the concentration distribution does not reach a steady state. When $\Phi = 0.05$, only a small change in the concentration is observed in the region $-|y_{th}| \leqslant y \leqslant |y_{th}|$, where $|y_{th}| \approx 12$. A layer of slightly high concentration appears around $y \approx 10$. When $\Phi = 0.125$, a larger concentration change is observed in the region $-|y_{th}| \leqslant y \leqslant |y_{th}|$, where $|y_{th}| \approx 31$. Because the effect of cell swimming increases as $\Phi$ is decreased, the accumulation of cells caused by cell swimming is enhanced as $\Phi$ is decreased. When $\Phi = 0.125$, a very thin layer of high cell concentration also appears near the upper wall. Thus, two layers of high concentration are evident in this case. When $\Phi = 0.167$, on the other hand, the concentration becomes large in the wide region $25 \leqslant y$, and a thick layer of high concentration appears near the wall. These results illustrate that the spatial distribution of cells in a Poiseuille flow is strongly dependent on the flow velocity.

In order to efficiently discuss the effect of cell swimming, we calculate the dimensionless average concentration $c^*_{out}$ and the concentration flux $q^*_{out}$ at the outlet at time $t\Phi = 100$. The definitions of $c^*_{out}$ and $q^*_{out}$ are

$$c^*_{out} = \frac{\displaystyle\int_{-H/2}^{H/2} c_{out}\, \mathrm{d}y}{\displaystyle\int_{-H/2}^{H/2} c^{ip}_{out}\, \mathrm{d}y}, \quad q^*_{out} = \frac{\displaystyle\int_{-H/2}^{H/2} c_{out} V_{x,out}\, \mathrm{d}y}{\displaystyle\int_{-H/2}^{H/2} c^{ip}_{out} V_{x,out}\, \mathrm{d}y}, \tag{4.2}$$

https://doi.org/10.1017/jfm.2012.116 Published online by Cambridge University Press

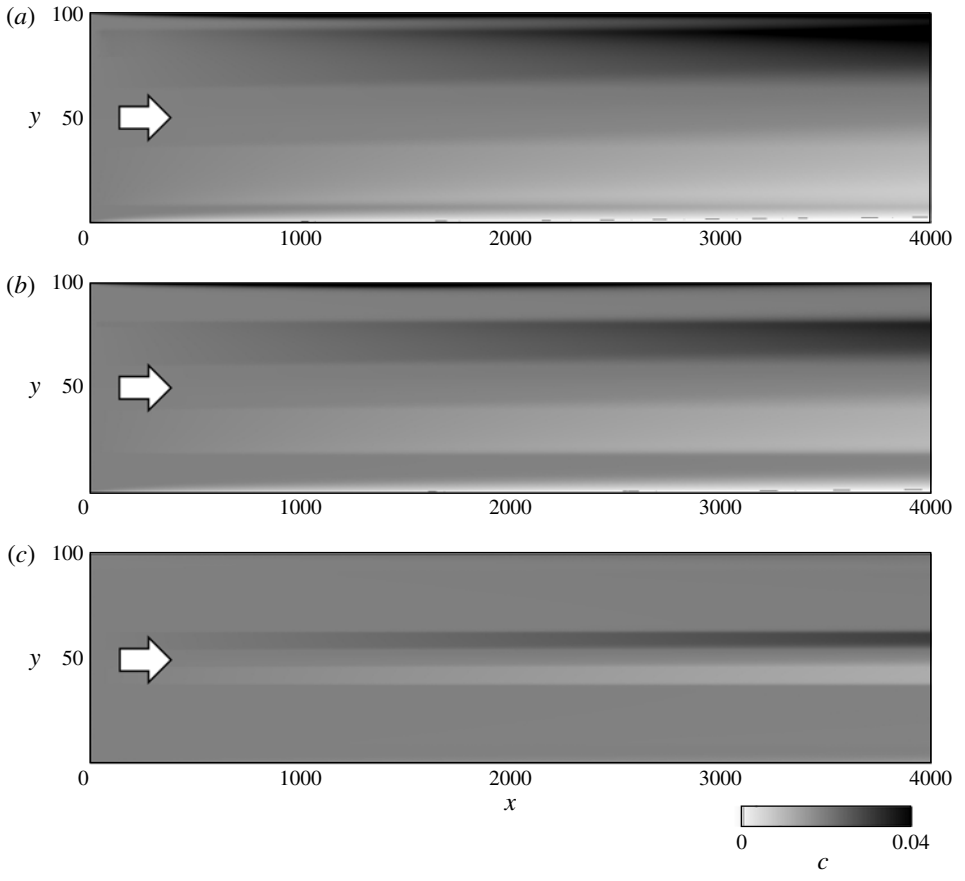



FIGURE 10. Two-dimensional concentration distributions in a horizontal Poiseuille flow at $t\Phi = 100$ ($\beta = 5$ and $\Phi\Psi = 0.2$). The white arrows indicate the flow direction: (*a*) $\Phi = 0.167$; (*b*) $\Phi = 0.125$; and (*c*) $\Phi = 0.05$.

where $c^{ip}$ is the reference concentration of inert particles that move with the same velocity as the background flow, without diffusion or drift (i.e. perfect tracers). This normalization makes the effect of cell swimming observable because the difference in $c_{out}$ and $c^{ip}_{out}$ is then due solely to cell swimming. The results for $c^*_{out}$ and $q^*_{out}$ are shown in figure 12. The value of $q^*_{out}$ is close to 1.0, which indicates that the concentration flux is not affected much by the swimming motion of the cells under constant inlet cell flux conditions. The value of $c^*_{out}$, on the other hand, is significantly larger than 1. If $\Phi$ is larger than 0.167, $c^*_{out}$ can increase greatly. Such computations are not performed, because high local concentrations appear in the computational domain before $t\Phi = 100$. Figure 12 illustrates the fact that the average concentration of cells at the outlet is significantly larger than that of inert particles, and the effect of cell swimming cannot be neglected. This is because the swimming cells accumulate near the upper wall, where the velocity is small, and the cell concentration becomes anisotropic. The volume fraction of bottom-heavy cells in a horizontal channel is therefore larger than the volume fraction in the inlet container.

Such an accumulation tendency is opposite to that of blood flow in a small tube, where the volume fraction of cells becomes smaller than that in the inlet container.

https://doi.org/10.1017/jfm.2012.116 Published online by Cambridge University Press

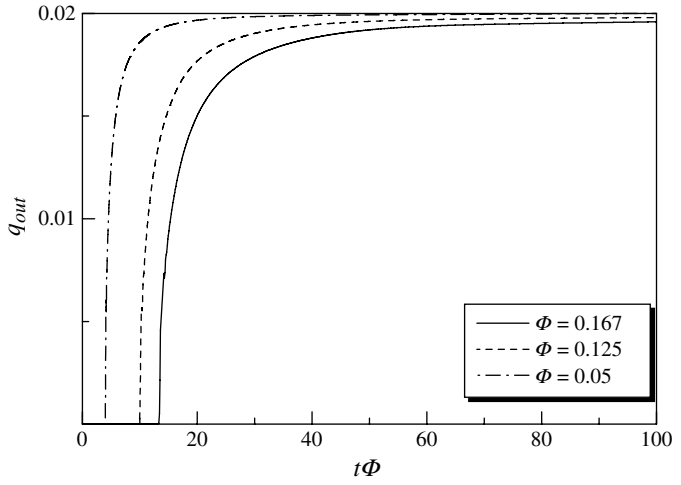



FIGURE 11. Changes in $q_{out}$ over time with $\Phi = 0.167$, 0.125 and 0.05 ($\beta = 5$ and $\Phi\Psi = 0.2$).

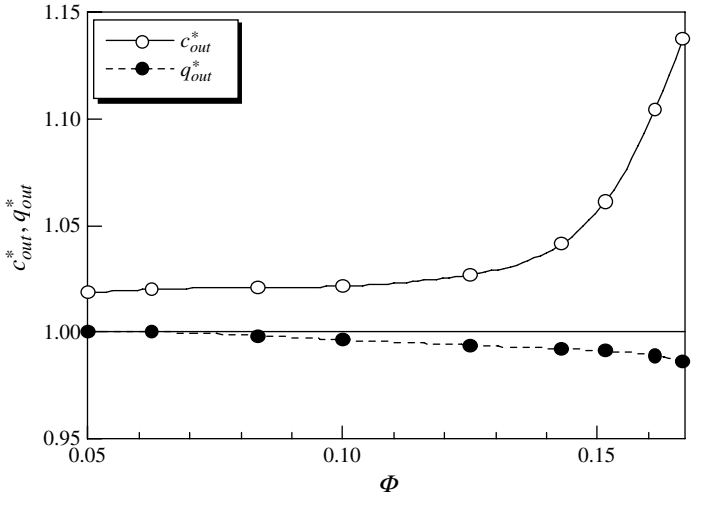



FIGURE 12. Effect of $\Phi$ on $c^*_{out}$ and $q^*_{out}$ at $t\Phi = 100$ ($\beta = 5$ and $\Phi\Psi = 0.2$).

This is known as the Fåhræus effect (Fåhræus 1929). Because of their deformability, red blood cells migrate toward the channel centre, where the velocity is high, whereas the gravitational torque of bottom-heavy microorganisms causes them to migrate toward the upper wall, where the velocity is low. Under constant inlet cell flux conditions, the difference between the migration positions of red blood cells and bottom-heavy cells results in the opposite tendency for the volume fraction of cells in the channel. These fundamental findings are helpful in understanding the distribution of microorganisms in various water regimes in nature and industry.

https://doi.org/10.1017/jfm.2012.116 Published online by Cambridge University Press

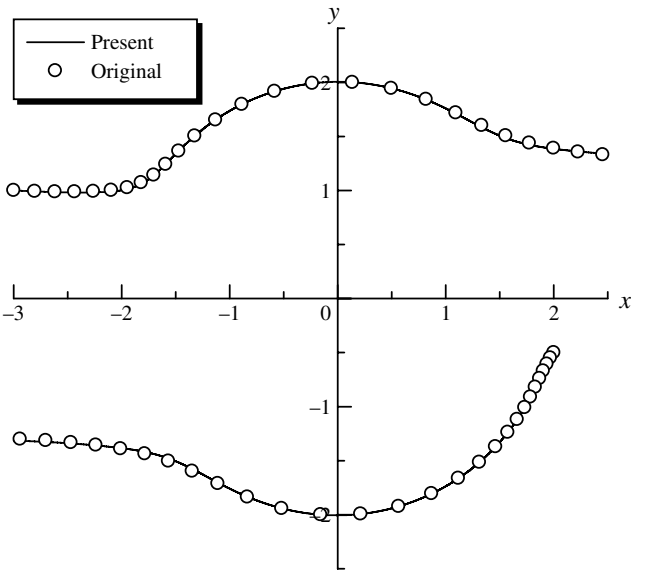



FIGURE 13. Trajectories of spheres A and C relative to B calculated by the present numerical method and the original method. Three spheres are placed initially at (−3, 1, 0), (0, 0, 0) and (2, −0.5, 0), and the background shear is applied using (2.8).

**Acknowledgements**

I would like to record my warm appreciation of the great pleasure that I derived from working with Professor T. J. Pedley since 2002. He has been a great mentor for me not only scientifically but also personally. I also acknowledge fruitful discussions on the present study with Professor T. J. Pedley and Dr J. T. Locsei. This paper was written under difficult circumstances after the earthquake and tsunami on 11 March 2011, in Japan. I truly appreciate the kind support of and encouragement from my colleagues, friends and family. This work was supported by the Funding Program for Next Generation World-Leading Researchers from the Japan Society for the Promotion of Science.

## Appendix A. Benchmark test: three spheres under shear flow

The aim of this appendix is to validate the numerical method used by comparing it with the original method reported by Ishikawa *et al.* (2008). The motion of three spheres in shear flow is calculated, and the trajectories are compared between the two numerical methods. This benchmark test clarifies the accuracy in the near-field interactions of a sheared suspension.

Three inert spheres, A, B, and C, were initially placed at (−3, 1, 0), (0, 0, 0), and (2, −0.5, 0), respectively. Then, the motion of the spheres in shear flow, given by (2.8), was calculated by the present method and the original method. The trajectories of spheres A and C relative to sphere B are shown in figure 13. As can be seen, the trajectories calculated by the two methods match perfectly. These results indicate that the present method has the same accuracy as the original method in calculating the near-field interactions of a sheared suspension.

https://doi.org/10.1017/jfm.2012.116 Published online by Cambridge University Press

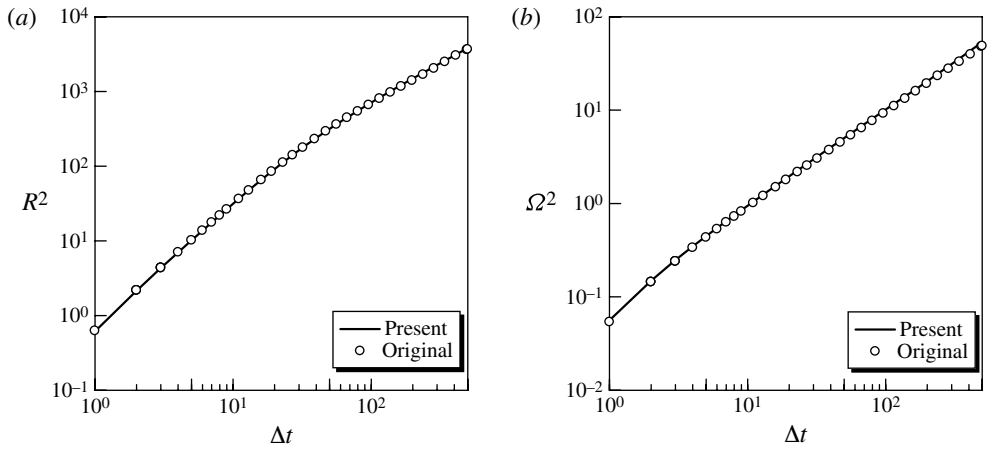



FIGURE 14. Square displacements of squirmers in a fluid otherwise at rest calculated by the present numerical method and the original method ($\beta = 5$ and $c = 0.1$): (*a*) translational square displacement; and (*b*) rotational square displacement.

## Appendix B. Benchmark test: diffusion of squirmers in a still fluid

The aim of this appendix is again to clarify the reliability of the present numerical method by comparing with the original method. The motion of squirmers in a fluid otherwise at rest is computed, and the square displacement is compared between two numerical methods. This benchmark test clarifies the accuracy in the far- and near-field interactions of squirmers in an infinite suspension.

A total of 64 NBH squirmers were initially placed in a cube with periodic boundary conditions with random positions and orientations. Then, the three-dimensional movement of squirmers in a fluid otherwise at rest was computed ($\beta = 5$ and $c = 0.1$). The results in terms of translational and rotational square displacements are shown in figure 14. The square displacements calculated by the two methods again match well. These results indicate that the present method has similar accuracy to the original method in calculating the far- and near-field interactions of squirmers in an infinite suspension.

## REFERENCES

BANCHIO, A. J. & BRADY, J. F. 2003 Accelerated Stokesian dynamics: Brownian motion. *J. Chem. Phys.* **118**, 10323.

BEARON, R. N., HAZEL, A. L. & THORN, G. J. 2011 The spatial distribution of gyrotactic swimming micro-organisms in laminar flow fields. *J. Fluid Mech.* **680**, 602–635.

BEENAKKER, C. W. J. 1986 Ewald sum of the Rotne–Prager tensor. *J. Chem. Phys.* **85**, 1581–1582.

BERG, H. C. 1983 *Random Walks in Biology*. Princeton University Press.

BRADY, J. F. & MORRIS, J. F. 1997 Microstructure of strongly sheared suspensions and its impact on rheology and diffusion. *J. Fluid Mech.* **348**, 103–139.

CHILDRESS, S., LEVANDOWSKY, M. & SPIEGEL, E. A. 1975 Pattern formation in a suspension of swimming micro-organisms: equations and stability theory. *J. Fluid Mech.* **63**, 591–613.

DRAZER, G., KOPLIK, J., KHUSID, B. & ACRIVOS, A. 2002 Deterministic and stochastic behaviour of non-Brownian spheres in sheared suspension. *J. Fluid Mech.* **460**, 307–335.

https://doi.org/10.1017/jfm.2012.116 Published online by Cambridge University Press

DURHAM, W. M., KESSLER, J. O. & STOCKER, R. 2009 Disruption of vertical motility by shear triggers formation of thin phytoplankton layers. *Science* **323**, 1067–1070.

DURHAM, W. M., CLIMENT, E. & STOCKER, R. 2011 Gyrotaxis in a steady vortical flow. *Phys. Rev. Lett.* **106**, 238102.

FÅHRÆUS, R. 1929 The suspension stability of the blood. *Physiol. Rev.* **9**, 241–274.

FOSS, D. & BRADY, J. F. 1999 Self-diffusion in sheared suspensions by dynamic simulation. *J. Fluid Mech.* **401**, 243–274.

FOSS, D. & BRADY, J. F. 2000 Structure, diffusion and rheology of Brownian suspensions by Stokesian Dynamics simulation. *J. Fluid Mech.* **407**, 167–200.

HILL, N. A. & HÄDER, D.-P. 1997 A biased random walk model for the trajectories of swimming micro-organisms. *J. Theor. Biol.* **186**, 503–526.

ISHIKAWA, T., SIMMONDS, M. P. & PEDLEY, T. J. 2006 Hydrodynamic interaction of two swimming model micro-organisms. *J. Fluid Mech.* **568**, 119–160.

ISHIKAWA, T. & PEDLEY, T. J. 2007 Diffusion of swimming model micro-organisms in a semi-dilute suspension. *J. Fluid Mech.* **588**, 437–462.

ISHIKAWA, T., LOCSEI, J. T. & PEDLEY, T. J. 2008 Development of coherent structures in concentrated suspensions of swimming model micro-organisms. *J. Fluid Mech.* **615**, 401–431.

ISHIKAWA, T. & YAMAGUCHI, T. 2008 Shear-induced fluid-tracer diffusion in a semi-dilute suspension of spheres. *Phys. Rev.* E **77**, 041402.

KESSLER, J. O. 1986 The external dynamics of swimming micro-organisms. In *Progress in Phycological Research* (ed. F. E. Round & D. J. Chapman), vol. 4, pp. 257–307. Biopress.

LEONARD, B. P. 1979 A stable and accurate convective modelling procedure based on quadratic upstream interpolation. *Comput. Meth. Appl. Mech. Engng* **19**, 59–98.

MARCHIORO, M. & ACRIVOS, A. 2001 Shear-induced particle diffusivities from numerical simulations. *J. Fluid Mech.* **443**, 101–128.

MORRIS, J. F. & BRADY, J. F. 1996 Self-diffusion in sheared suspensions. *J. Fluid Mech.* **312**, 223–252.

SIEROU, A. & BRADY, J. F. 2004 Shear-induced self-diffusion in non-colloidal suspensions. *J. Fluid Mech.* **506**, 285–314.

VLADIMIROV, V. A. *et al*. 2000 Algal motility measured by a laser-based tracking method. *Mar. Freshwat. Res.* **51**, 589–600.

VLADIMIROV, V. A. *et al*. 2004 Measurement of cell velocity distributions in populations of motile algae. *J. Expl Biol.* **207**, 1203–1216.

WANG, Y., MURAI, R. & ACRIVOS, A. 1998 Transverse Shear-induced gradient diffusion in a dilute suspension of spheres. *J. Fluid Mech.* **357**, 279–287.

https://doi.org/10.1017/jfm.2012.116 Published online by Cambridge University Press